Research Article

Journal of RAMAN SPECTROSCOPY

Received: 2 October 2009 Accepted: 7 February 2010 Published online in Wiley Interscience:

(www.interscience.wiley.com) DOI 10.1002/jrs.2647

Fast three-dimensional chemical imaging by interferometric multiplex coherent anti-Stokes Raman scattering microscopy

Jiha Sung, Bi-Chang Chen and Sang-Hyun Lim*

We report significant improvements in both signal sensitivity and imaging speed of Fourier transform spectral interferometry coherent anti-Stokes Raman scattering (FTSI-CARS) microscopy. With a help of an apodization function in the signal retrieval process, background due to the spectral change of nonresonant signals is eliminated. We experimentally verify that the sensitivity of the improved method is nearly shot-noise-limited. The current maximum detection sensitivity is ~10 mM of aqueous sulfate ions, which correspond to ~10^6 oscillators in the microscopy focal volume. Operating the charge-coupled device (CCD) in the crop mode increases the image acquisition speed by more than ten times. A vibrational hyperspectral image of a polymer sample with 100 × 100 pixel can be obtained within 3 s. With the improved sensitivity and speed, we also perform three-dimensional volume imaging. Superior chemical selectivity is demonstrated with a mixture of two different oil droplets, which have identical vibrational peak positions but different relative peak ratios.

Keywords: FTSI-CARS; CARS microscopy; sensitivity; shot-noise-limit; chemical imaging

Introduction

Over the last decade, coherent anti-Stokes Raman scattering (CARS) microscopy has progressed greatly and become a powerful imaging tool in biology and material science.[1,2] Its intrinsic vibrational image contrast with great signal sensitivity provides a fast label-free three-dimensional (3D) chemical imaging modality, which is highly desirable for the study of complex inhomogeneous samples such as living cells.[2–5] The CARS microscopy technique employing narrow bandwidth lasers has proven to be an excellent tool for lipid imaging thanks to the isolated vibrational frequency of the C–H stretching mode and its abundance in long lipid alkyl chains.[6–12] However, chemical imaging of non-lipid samples with the narrowband CARS method has been challenging. The vibrational fingerprint region, where one can find characteristic vibrational response of most organic molecules, is often crowded with many overlapping peaks and spectral analysis is typically required to distinguish the sample against other molecules.[13,14] Although vibrational spectrum can be obtained by tuning the frequency of one laser in the narrowband CARS method, it is a slow and tedious process in general.[6,9] Fluctuations of samples and laser power are also significant problems in this approach.

A complete vibrational spectrum can be obtained in a single measurement by multiplex CARS techniques.[13–22] Here, broadband laser pulses excite multiple vibrational peaks simultaneously and a narrowband probe pulse generates CARS spectrum in a single measurement.[14,15,21] The multiplex CARS technique provides greater chemical selectivity than the narrowband CARS method since it enables full vibrational analysis.[15–20,23–27] Recently, we have developed the Fourier transform spectral interferometry CARS (FTSI-CARS) technique, an interferometric multiplex CARS technique that can obtain Raman-like vibrational spectrum of sample molecules by manipulating the spectral amplitude and phase of a single broadband laser pulse.[15,19]

In our previous report,[15] it has been demonstrated that a vibrational spectrum from liquid and polymer samples can be obtained with a charge-coupled device (CCD) exposure time of 20–100 μs. However, the data transfer speed was much slower (around 2 ms per spectrum) and the total image acquisition time was limited to ~40 s for 100 × 100 pixel images.[15] We also find that nonresonant background, which we use as a local oscillator for spectral interferometry to extract the CARS spectrum, can vary over sample positions as a result of the change of optical alignment and the different electronic response of local samples. This creates undesired background in the resulting FTSI-CARS spectra.[28]

In this work, we report that this background due to spectral nonuniformity of the nonresonant background can be eliminated by introducing a time apodization function in the FTSI process, thus improving sensitivity of this method. Nearly shot-noise-limited Raman-like spectrum can be obtained over entire 900–1600 cm^{-1} wavenumber range. CCD data transfer speed is also significantly increased by operating the CCD in the so-called crop mode. We show that a vibrational hyperspectral image of 100 × 100 pixels can be obtained in 3 s, which is more than ten times faster than the speed reported in our previous work. 3D volume imaging of 100 × 100 × 50 pixels can be completed in 3 min. Chemical imaging of polymer and edible oil samples are performed to demonstrate the capability of the improved technique.

* *Correspondence to: Sang-Hyun Lim, Department of Chemistry and Biochemistry, University of Texas at Austin, 1 University Station A5300, Austin, TX 78712, USA. E-mail: shlim@mail.utexas.edu*

Department of Chemistry and Biochemistry, University of Texas at Austin, 1 University Station A5300, Austin, TX 78712, USA

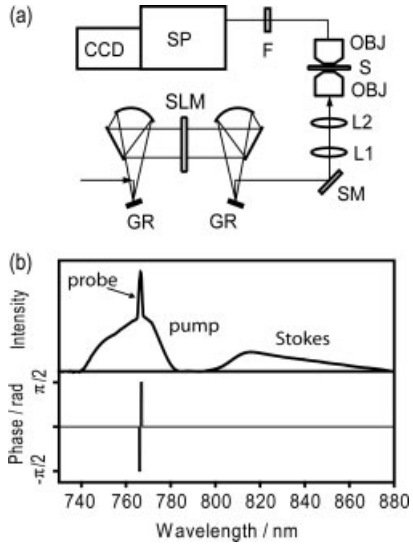

Figure 1. (a) Experimental setup: GR, grating; SLM, liquid crystal spatial light modulator; SM, beam scanning mirror; L1, scan lens; L2, tube lens; OBJ, microscope objective; S, sample on XYZ stage; F, short-wavelength-pass filter; SP, spectrometer. (b) Intensity and phase spectra of the CARS laser pulse used in FTSI-CARS experiments.

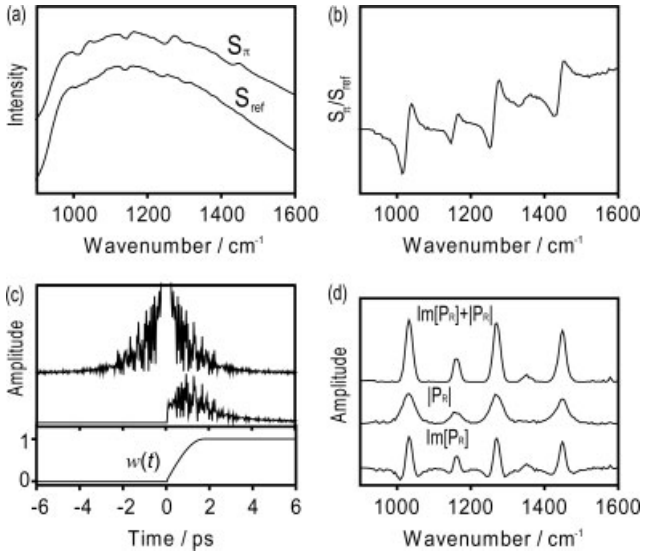

Figure 2. Signal retrieval procedure of FTSI-CARS. (a) Measured CARS signals from cyclohexane by the CARS (S_π) and reference (S_{ref}) laser pulses. (b) Normalized CARS signal (S_π/S_{ref}). (c) FT of the normalized signal (top), time profile after applying apodization function (middle) and the apodization function ($w(t)$) (bottom). (d) Imaginary part (bottom), amplitude (middle) and a sum of the imaginary part and amplitude (top) of the inverse FT of the middle trace in (c). The traces in panels (a), (c) and (d) are vertically displaced for clarity. The CCD exposure time is 2 ms.

Experimental

Figure 1(a) shows our experimental setup.[15] We use single broadband pulses from a cavity-dumping Ti : sapphire oscillator (Cascade, KM Lasers) to generate the CARS signals.[15] The output power of this laser is 40 nJ at a repetition rate of 2 MHz. The amplitude and phase of the laser pulse are controlled by an all reflective 4*f* pulse shaper using a 640-pixel dual-bank liquid crystal spatial light modulator (SLM-640, CRI). The wavelengths of the laser shorter than 740 nm are blocked by a razor blade placed at the Fourier plane of the pulse shaper. Figure 1(b) shows the intensity and phase spectra of the shaped laser pulse after the pulse shaper. Note that all the pump, Stokes, and probe pulses are chosen from a single broadband laser pulse. For the spectroscopy of liquid samples, the powers of pump, Stokes, and probe pulses are set to 2.0, 1.0, and 0.3 mW, respectively. For microscopy of polymers and oil droplets, adequate powers for each pulse are chosen below the damage threshold of each sample. The spectral resolution of the pulse shaper is 0.4 nm, which corresponds to 5.3 cm^{-1} at 800 nm. The probe pulse is selected with four SLM pixels, which corresponds to a bandwidth of 21 cm^{-1}. The shaped laser pulse is focused onto a sample by a 1.2 numerical aperture (NA) water immersion microscope objective lens (Olympus). The CARS signals are collected by a 1.0 NA water immersion objective lens (Olympus), filtered by a sharp-edge short-wavelength-pass filter (710ASP, Omega Optical) and directed to a spectrometer (Holospec *f*/1.8, Kaiser Optical Systems) equipped with a frame-transfer, back-illuminated CCD camera (DV887, Andor). The spectral phase of the laser pulse at the sample position is characterized and compressed by the single-beam homodyne spectral phase interferometry for direct electric field reconstruction (SPIDER) technique developed by our group previously.[29]

Raman-like CARS spectra are obtained by the FTSI-CARS method by the following procedure.[15] CARS ($S_\pi(\omega)$) and reference ($S_{ref}(\omega)$) signals are generated by the CARS and reference pulses, respectively. The amplitude and phase structure of the CARS pulse is depicted in Fig. 1(b). The reference pulse is transform-limited and does not have the π step-phase at the probe frequency. Identical amplitude masks are used for both CARS and reference pulses. $S_\pi(\omega)$ is normalized with $S_{ref}(\omega)$, Fourier transformed, multiplied by an apodization function $w(t)$ [shown in Fig. 2(c)], and inverse-Fourier-transformed to generate the vibrational CARS spectra. Details of the signal retrieval procedure and the role of the newly introduced apodization function are presented in the following section.

Hyperspectral vibrational imaging is performed by moving both the laser beam and the sample stage. While the laser beam is scanned along one axis (*y*-axis) by a piezo-driven scanning mirror [SM in Fig. 1(a), S-334.2SL, PI], the sample stage (P-542.2SL, PI) is translated along the perpendicular axis (*x*-axis). 3D imaging is performed by moving the sample vertically by a motorized actuator (Z606, Thorlabs). Currently, our CCD camera can measure full vertical binned spectra with an exposure time as short as 20 µs without a mechanical shutter. However, the data transfer speed of our CCD is much slower; the maximum data transfer speed of our CCD is ~2 ms per spectrum. We operate the CCD in the kinetic mode to acquire the entire spectra along one line (*y*-axis) of the image by a single command. This method minimizes the number of command sets and speeds up the data transfer significantly. The laser beam scanning is synchronized with the CCD TTL output to ensure that the scanning laser spot position is correlated with the measured spectrum. After acquiring one line of the image, the sample is moved to the next *x*-axis point and this process is repeated until the full image is acquired. The entire 2D data are then processed with the FTSI algorithm described in a later section. The data transfer speed can be improved further via the crop mode operation. We set the CCD to read only 128 rows out of the original 512 rows to maximize CCD readout speed. In this condition, the maximum CCD speed of 250 µs per spectrum can be achieved with 3 MHz CCD clock frequency. With 200 µs exposure time per pixel, a 100 × 100 pixel image can be obtained in 3.4 s, which includes

the CCD exposure, data transfer, and FTSI numerical process. This speed is 13 times faster than that in our previous report. We run the experiments with a homemade program written in the Labview 8.2 program language with the software development kit from the CCD manufacturer (Andor SDK, version 4.83).

Liquid samples are prepared by sandwiching a small drop of the liquid between two microscope coverslips. Polymer mixture samples are prepared by melting polystyrene (PS) and polyethylene terephthalate (PET) powders on top of a glass substrate. Oil droplet is prepared by the following method. Olive or fish oil (0.05 g) purchased from a local grocery store is mixed with 0.05 g of Triton X-100 (Sigma-Aldrich) and stirred for 5 min. Six milliliters of water is added to the mixture and stirred further for 2 h. Separately prepared olive and fish oil droplet samples are mixed and a small drop from the mixture is sandwiched between two microscope coverslips.

Results and Discussion

FTSI-CARS and time apodization function

Figure 2 describes the new FTSI-CARS procedure. The experimental CARS and reference signals from cyclohexane are shown in Fig. 2(a). S_π is obtained with the CARS pulse as depicted in Fig. 1(b). Note that the π-step phase is applied in the narrow probe region. The probe pulse with π-step phase does not excite coherent vibrations and eliminates any complication from vibrational excitation by the probe pulse.[19,21,22] S_{ref} is generated by a transform-limited reference excitation laser, which does not have the π-step phase structure.[19] With all the samples that we have tested by our method so far, we find that nonresonant background is always much larger than resonant CARS signal. In this situation, the measured CARS signal ($S_\pi(\omega)$) becomes[21]

$$S_\pi(\omega) \propto |P_{\text{NR}}(\omega) + P_{\text{R}}(\omega)|^2 \approx P_{\text{NR}}(\omega)^2 + 2P_{\text{NR}}(\omega)Re[P_{\text{R}}(\omega)] \quad (1)$$

where $P_{\text{NR}}(\omega)$ and $P_{\text{R}}(\omega)$ are the polarizations of the nonresonant background and spectrally resolved resonant signal generated by phase-shaped probe pulse, respectively. ω is the frequency. Note that $P_{\text{NR}}(\omega)$ is purely real. The cross-term $P_{\text{NR}}(\omega)$ Re$[P_{\text{R}}(\omega)]$ can be obtained by normalizing the CARS signal $S_\pi(\omega)$ with the reference signal S_{ref}. The normalized signal becomes

$$S_\pi(\omega)/S_{\text{ref}}(\omega) \approx \left|\frac{P_{\text{NR}}(\omega)}{P^0_{\text{NR}}(\omega)}\right|^2 + \frac{2P_{\text{NR}}(\omega)}{\left|P^0_{\text{NR}}(\omega)\right|^2}\text{Re}[P_{\text{R}}(\omega)] \quad (2)$$

where $P^0_{\text{NR}}(\omega)$ is the polarization of the nonresonant background generated by the reference excitation pulse. The first term in Eqn (2) ($|P_{\text{NR}}(\omega)/P^0_{\text{NR}}(\omega)|^2$) gives a constant offset and the nonresonant contribution in the second term ($P_{\text{NR}}(\omega)/|P^0_{\text{NR}}(\omega)|^2$) also has a much smoother ω dependence compared to Re$[P_{\text{R}}(\omega)]$. As a result, $S_\pi(\omega)/S_{\text{ref}}(\omega)$ has the spectral line shape of the real part of the resonant CARS polarization as one can see in Fig. 2(b). Note that S_{ref} in Fig. 2(a) is not perfectly smooth and shows small fringes due to the etalon effect of CCD and non-flat transmission spectrum of the filter that is used to block the laser pulse. We use a back-illuminated CCD since it has about twice higher sensitivity than front-illuminated one. However, nearly parallel front and back surfaces of the CCD chip cause the etalon effect, especially when it is used in the near infrared (NIR) region. It creates fringe artifacts in the signal spectrum as one can see in Fig. 2(a). This signal distortion can be completely removed by the normalization process of Eqn (2) as one can see in Fig. 2(b). Since both the etalon and filter transmission effects are identical on S_{ref} and S_π, the normalized CARS signal with the reference signal is free from such artifacts. This is an important issue in multiplex CARS experiments with weak signal samples. Small CARS signals can be easily buried in such artifacts since their frequency spacing is close to that of the vibrational signature in the measured signals.

In our previous work, $P_{\text{R}}(\omega)$ was retrieved by the Fourier transform (FT) of Re$[P_{\text{R}}(\omega)]$ utilizing the causality principle of vibrational excitation:[15,19]

$$\text{FT}^{-1}\,[\theta(t)\text{FT}[\text{Re}[P_{\text{R}}(\omega)]]] = P_{\text{R}}(\omega) \quad (3)$$

In this work, we use an apodization function ($w(t)$) instead of Heaviside step function ($\theta(t)$), that is:

$$\text{FT}^{-1}\,[w(t)\text{FT}[\text{Re}[P_{\text{R}}(\omega)]]] = P_{\text{R}}(\omega) \quad (4)$$

and $w(t)$ is defined by

$$\begin{aligned} w(t) &= 0, \text{ when } t < 0 \\ &= \sin\left(\frac{\pi}{2\tau}t\right), \text{ when } 0 \le t \le \tau \\ &= 1, \text{ when } t > \tau \end{aligned} \quad (5)$$

where τ is an appropriate time constant. The bottom trace in Fig. 2(c) shows the shape of $w(t)$. The top trace of Fig. 2(c) is FT of the normalized signal ($S_{pi}(\omega)/S_{\text{ref}}(\omega)$). The time trace after applying $w(t)$ is shown in the middle plot of Fig. 2(c). For all FTSI-CARS spectra in this report, $\tau = 1.77$ ps is used. The apodization function ($w(t)$) not only cuts out time trace before $t = 0$, but also rounds off the trace close to $t = 0$. We choose $w(t)$ in the form of Eqn (5) for its simplicity. Figure 2(d) shows the imaginary part, amplitude, and the sum of the imaginary part and amplitude from the inverse FT of the time trace shown in the middle plot of Fig. 2(c). All the spectra in later discussion are Im$[P_{\text{R}}] + |P_{\text{R}}|$, which shows a Raman-like spectral shape.[15]

Liu *et al*. pointed out that the change of the spectral shape of the nonresonant background cannot be compensated by simple normalization and it can adversely impact the spectral feature of the retrieved CARS vibrational spectrum.[28] The change of nonresonant background can occur because of fluctuation of the laser spectral shape during the image acquisition, the change of optical alignment, and different electronic resonances of local samples. Figure 3 shows how such different spectral shapes of nonresonant backgrounds in S_π and S_{ref} affect the extracted CARS spectrum. In the experiment of Fig. 3, we intentionally change the spectral shape of the nonresonant background in the reference signals by applying a different amplitude mask to the reference laser pulse. The measured CARS and reference signals from cyclohexane by the original CARS and distorted reference laser pulses, respectively, are shown in Fig. 3(a). Note that the resulting reference signal ($S_{\text{ref,dist}}$) has a very different spectral shape from the one by the original reference laser pulse [S_{ref} in Fig. 2(a)]. One can see a significant distortion of $S_\pi(\omega)/S_{\text{ref,dist}}(\omega)$ in Fig. 3(b). Figure 3(c) shows the time profiles obtained by FT and multiplication of $\theta(t)$ [top trace of Fig. 3(c)] and the apodization function ($w(t)$) [bottom trace of Fig. 3(c)], respectively. The retrieved CARS spectra are shown in Fig. 3(d). The CARS spectrum with $\theta(t)$ exhibits a significant background feature [top trace in Fig. 3(d)]. Although this background is smooth

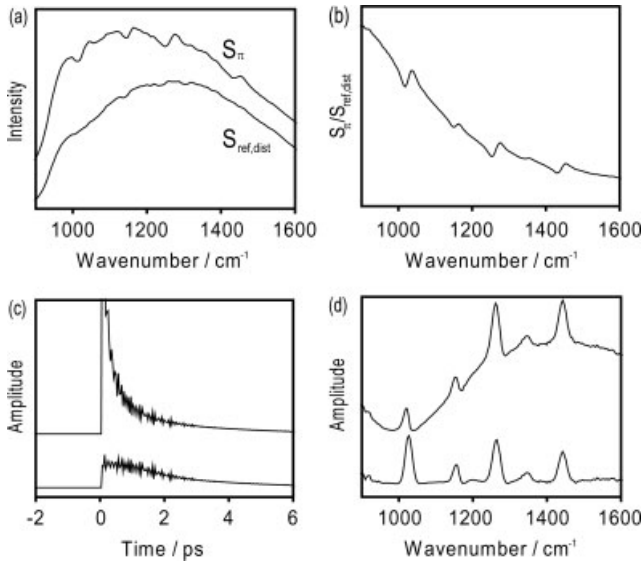

Figure 3. (a) Measured CARS signals from cyclohexane by the CARS (S_π, top) and distorted reference pulses ($S_{ref,dist}$, bottom). (b) Normalized CARS signal ($S_\pi/S_{ref,dist}$). (c) FT of the normalized signal multiplied by the Heaviside step function (top) and the apodization function (bottom). (d) Retrieved CARS spectra with the Heaviside step function (top) and with the apodization function (bottom). The traces in panels (a), (c), and (d) are vertically displaced for clarity. The CCD exposure time is 2 ms.

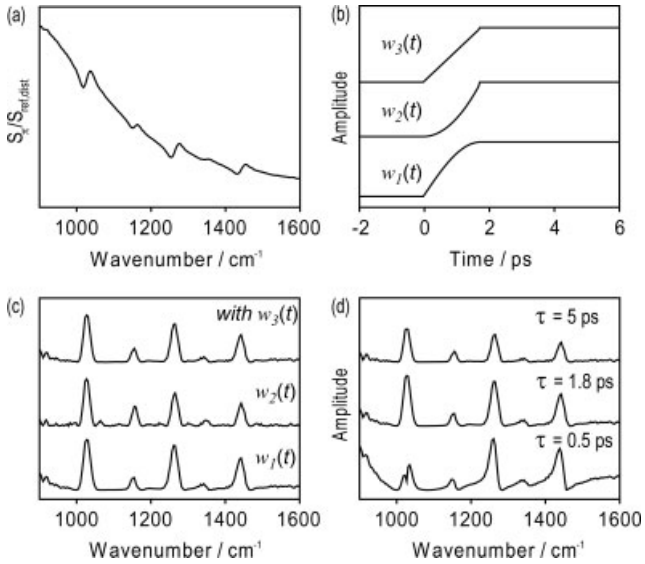

Figure 4. Effect of the shape of the apodization function. (a) Distorted normalized CARS signal from Fig. 3(b). (b) Three different apodization functions; $w_1(t) = \sin(\pi t/2\tau)$, $w_2(t) = (t/\tau)^2$, and $w_3(t) = t/\tau$ over $0 \leq t \leq \tau$. (c) Retrieved CARS spectra using $w_1(t)$, $w_2(t)$, and $w_3(t)$ as apodization functions. $\tau = 1.8$ ps. (d) Retrieved CARS spectra using $w_1(t)$ with $\tau = 0.5$, 1.8, and 5 ps. The traces in panels (b), (c), and (d) are vertically displaced for clarity.

compared to the vibrational peaks, it can still be a significant problem especially for weak vibrational peaks. This background can be removed by introducing $w(t)$. The bottom trace of Fig. 3(d) shows the retrieved CARS spectrum with $w(t)$. The background caused by the distorted reference signal is almost completely removed and the retrieved vibrational spectrum is essentially identical to the top trace of Fig. 2(d). The change in spectral shape of the nonresonant background is much smoother than that of vibrational signatures in the measured CARS signals. This results in sharp features around $t = 0$, and applying a smooth apodization function ($w(t)$) in the time domain can eliminate such background distortion.

One may remove the background by subtracting a polynomial background. However, it takes significant time to perform polynomial background subtraction from 10 000 such spectra without *a priori* knowledge of vibrational peak shapes. One must also examine each vibrational spectrum carefully to select the background frequency positions. Application of a time apodization function automates the background subtraction procedure and enables fast imaging processes.

We find that the shape of the apodization function does not affect the retrieved CARS spectrum significantly. Figure 4 shows the effect of the shape of the apodization function on the resulting CARS spectrum. We retrieve the FTSI-CARS spectrum from the distorted normalized CARS signal (Fig. 4(a)) with three different apodization functions (Fig. 4(b)) of $w_1(t) = \sin(\pi t/2\tau)$, $w_2(t) = (t/\tau)^2$, and $w_3(t) = t/\tau$ over $0 \leq t \leq \tau$. Figure 4(c) shows the retrieved CARS spectra using $w_1(t)$, $w_2(t)$, and $w_3(t)$ as apodization functions. Although $w_2(t)$ distorts the resulting CARS spectrum slightly [middle trace in Fig. 4(c)], all three apodization functions yield satisfactory CARS spectra. We also test other types of apodization functions to establish that the detailed shape of the apodization function is not important as long as it has a smooth shape. In the other hand, the choice of τ value is important. Figure 4(d) shows the effect of τ value with $w_1(t) = \sin(\pi t/2\tau)$. If it is too small, the background is not removed completely and spectral shapes of vibrational peaks are also distorted as one can see in the bottom trace of Fig. 4(d) ($\tau = 0.5$ ps). If it is too large, the intensity of the retrieved CARS signal decreases [top trace of Fig. 4(d), $\tau = 5$ ps]. We find that the optimal τ value is the vibrational dephasing time, which one can obtain from the linewidth of vibrational peaks. Thus, we use $\tau = 1.77$ ps in this work. This value is close to the vibrational dephasing time of typical organic molecules at room temperature.

Sensitivity of FTSI-CARS

We test the sensitivity of our FTSI-CARS technique with the 972 cm^{-1} peak of sulfate ions in an aqueous Na_2SO_4 solution. FTSI-CARS spectra are measured with various concentrations of Na_2SO_4 in solution. The acquisition time for each spectrum in Fig. 5 is 2 s. Figure 5(a) shows the FTSI-CARS spectra of 1 M, 125 mM, and 15.6 mM Na_2SO_4 solutions. The spectrum of water is also shown as a reference. Note that the spectrum of 1 M solution is scaled by a factor of 0.2 for clarity. The 970 cm^{-1} vibrational peak can be observed at a concentration down to 15.6 mM. At this concentration level, there are 1.2×10^6 sulfate ions in the focal volume of the laser focus. We estimate the focal volume of our microscope as 1.3×10^{-16} l, which is calculated from a diffraction-limited Gaussian laser beam profile. This vibrational peak is buried under noise at a concentration below 10 mM. We also test the detection limit of nitrate ions at the vibrational peak of 1037 cm^{-1} and find similar sensitivity (data not shown).

In the case of the homodyne limit (i.e.$P_{NR} << P_R$), the measured CARS signals ($S(\omega) \propto |P_{NR}(\omega) + P_R(\omega)|^2$) are dominated by $|P_R|^2$. In this regime, one observes quadratic dependence of the CARS signal.[2,30] In the heterodyne limit (i.e.$P_{NR} >> P_R$), where the condition of our technique occurs, we essentially measure the cross-term (P_{NR} Re[P_R]) that is linearly proportional to the sample

Journal of RAMAN SPECTROSCOPY

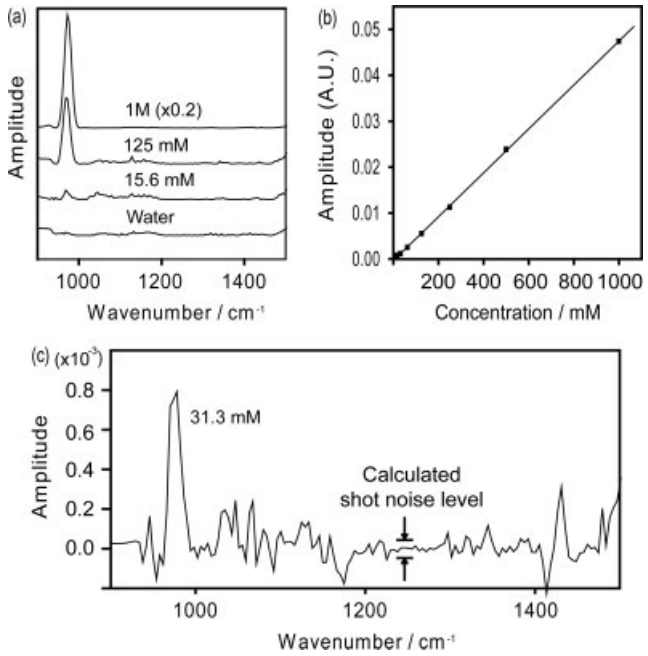

Figure 5. (a) FTSI-CARS spectra from an aqueous Na_2SO_4 solution of 1 M, 125 mM, and 15.6 mM concentrations. CARS spectrum of water is also shown (bottom). The CCD exposure time is 2 s and the spectrum of the 1 M solution is multiplied by a factor of 0.2. Each trace is vertically displaced for clarity. (b) Concentration dependence of FTSI-CARS intensity of Na_2SO_4 aqueous solution. (c) FTSI-CARS spectrum of 31 mM aqueous Na_2SO_4 solution. A shot noise level calculated from total photoelectron count is marked with arrows. See text for details.

concentration. The linear concentration dependence of the FTSI-CARS intensity is obvious in Fig. 5(b), which confirms the signal amplification by the nonresonant background in our FTSI-CARS technique.

The main noise source in the measured CARS signal is the shot noise from nonresonant background [P_{NR}^2 in Eqn (1)]. The standard deviation (σ) of the quantum fluctuation of the nonresonant background (i.e. shot noise) becomes P_{NR} from the Poison distribution (i.e. $\sigma = P_{NR}$). Our FTSI-CARS method retrieves the cross-term ($P_{NR}P_R$), and the signal-to-noise ratio (SNR) is estimated as

$$\mathrm{SNR} = \frac{\mathrm{Signal}}{\mathrm{Noise}} = \frac{P_{NR}P_R}{P_{NR}} = P_R \qquad (6)$$

As such, our FTSI-CARS method is shot-noise-limited in theory. In the previous section, it was shown that the spectral noise from the etalon effect of CCD, imperfection of filter, laser drift, and sample fluctuation could be effectively removed by FTSI-CARS technique. Then, it is worth verifying how close its detection sensitivity is to the theoretical shot-noise-limit. We estimate the shot noise level (σ) in the following way. We first convert the experimental signal count in the measured signal spectrum to the number of photoelectrons (N) at every vibrational frequency. Then, we calculate the standard deviation of quantum fluctuation as $\sqrt{N}$. This noise appears as fluctuation of background via $\sqrt{N}/N = 1/\sqrt{N}$ because our extracted CARS spectrum is the ratio of the resonant signal over the dominant nonresonant background (N). In Fig. 5(c), the FTSI-CARS spectrum of an aqueous solution of Na_2SO_4 (31 mM) is shown with the calculated shot noise level (σ) of $\pm 4.5 \times 10^{-5}$. At the wavenumber of 1250 cm^{-1}, the number of measured photoelectrons of the raw data (N) is $\sim 5 \times 10^8$ and we obtain the above shot noise value. The measured background noise is very close to the estimated shot noise level, confirming that our FTSI-CARS method is almost shot-noise-limited.

2D and 3D chemical imaging of polymer mixture

Figure 6(a) and (b) shows chemically selective images of a PS/PET mixture film. The full vibrational spectra over 800–1700 cm^{-1} are obtained at every 100 × 100 pixels. The two CARS spectra at the positions A and B in Fig. 6(a) and (b) are shown in Fig. 6(c). The images are constructed by integrating 980–1020 cm^{-1} for PS and 1590–1640 cm^{-1} for PET out of 10 000 vibrational spectra. One can clearly see that the circular PS domains are surrounded by the PET matrix. The powers of the pump, Stokes, and probe pulses are 0.9, 0.9, and 0.3 mW, respectively. CCD exposure time per pixel is 200 μs and the total image acquisition time is 3.4 s. The total CCD exposure time for 10 000 spectra is 2 s, but the data transfer and FTSI numerical process take an additional 1.4 s. Note that the acquisition time for an image of 100 × 100 pixels was 43 s in our previous publication. We increased the image acquisition rate by more than 10 times with a help of the crop mode CCD operation. We find that this faster operation of the CCD significantly increases electronic noise but it does not affect the sensitivity of retrieved CARS signal due to the heterodyne signal amplification mechanism. For chemical imaging, we take the nonresonant CARS spectrum once at an arbitrary position and use it as a reference for the entire imaging. In the previous section, we demonstrated that the change of the spectral shape of nonresonant background creates a slowly varying background feature at the retrieved spectrum. Any drift of the laser spectrum during the imaging process and/or different electronic response at local samples adversely decreases the sensitivity of our method. This problem is virtually eliminated by applying the apodization function instead of the Heaviside step function. As a result, we can obtain the chemical image of a polymer sample in a much shorter time than in our previous demonstration.

With capability of a faster imaging speed, we can obtain a 3D volume image in a few minutes. Figure 7(a) shows a 3D volume image of the PS domains in the PS/PET film. The imaged area is 10 × 10 × 10 μm^3 and the entire vibrational spectra are taken at every 100 × 100 × 50 pixels (each pixel size is 100 × 100 × 200 nm^3). Total 5 × 10^5 spectra are obtained during the image acquisition time of 183 s, and the PS domains (the area where the 1000 cm^{-1} peak intensity is above 25% of the maximum intensity) are depicted with yellow contour surfaces. Figure 7(b) shows a sectioned image at z = 5 μm. The sectioned plane is shown with white lines in Fig. 7(a).

Chemical imaging of oil mixture

We also test the chemical selectivity of our method for identifying chemical species with similar vibrational spectra. Olive and fish oil droplets are chosen because they have very similar vibrational peak positions in the fingerprint region. The only difference between these two oil samples is the relative peak ratios. Figure 8(a) shows FTSI-CARS spectra of bulk fish and olive oil samples. The vibrational bands at 1260 and 1300 cm^{-1} are assigned to the =C–H in-plane deformation mode of an unsaturated *cis* double bond and the CH_2 twisting mode of a saturated C–C chain, respectively. As the degree of unsaturation increases, the peak intensity at 1260 cm^{-1} increases, while the one at 1300 cm^{-1} decreases. Therefore, the intensity ratio between these two vibrational peaks is a good measure of the unsaturation level of fatty acids.[31,32]

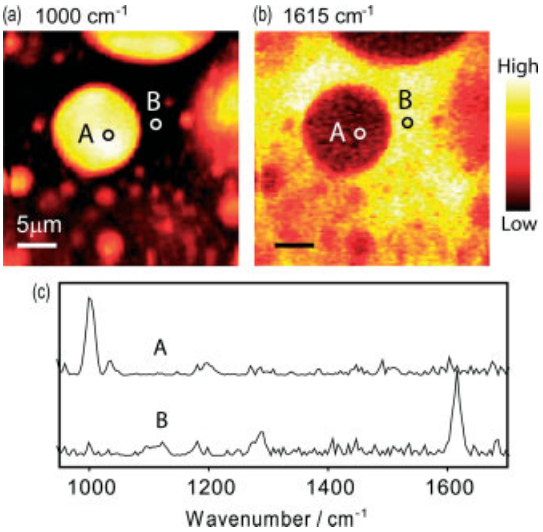

Figure 6. (a) and (b) Chemical imaging of the PS and PET polymer mixture film. Images are constructed with peaks at (a) 1000 cm^{-1} (PS) and (b) 1615 cm^{-1} (PET), respectively. The images have 100 × 100 pixels with the pixel size of 300 × 300 nm^2. The total image acquisition time is 3.4 s. (c) Two representative CARS spectra at position A and B in panels (a) and (b). These spectra are two out of 10 000 such spectra obtained during the image acquisition.

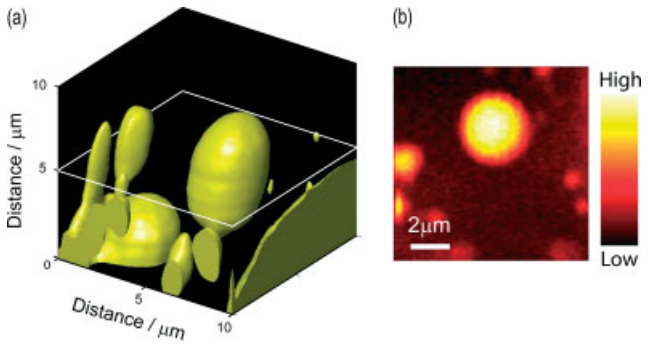

Figure 7. (a) 3D volume image of the PS and PET mixture film. PS domains are depicted with yellow contour surface. The image has 100 × 100 × 50 pixels with the pixel size of 100 × 100 × 200 nm^3. The total image acquisition time is 183 s. (b) Horizontally sectioned image at $z = 5$ μm [white line in panel (a)]. The image is constructed with the 1000 cm^{-1} peak of PS.

According to the manufacturer's label of the olive oil brand used in this experiment, it contains 14, 14, and 72% of saturated, polyunsaturated, and monounsaturated fatty acid, respectively. The major component in olive oil is oleic acid, which is a monounsaturated omega-9 fatty acid with an 18-carbon chain and one C═C double bond (18 : 1). For the fish oil, 50% of its content is a mixture of eicosapentanoic acid (20 : 5), docosahexanoic acid (22 : 6), and other polyunsaturated fatty acids according to the manufacture's label. The low unsaturation level of olive oil shows $I_{1260}/I_{1300} < 1$ where I_{1260} and I_{1300} are the peak intensities at 1260 and 1300 cm^{-1}, respectively. On the other hand, the high unsaturation level of fish oil exhibits $I_{1260}/I_{1300} > 1$, as shown in Fig. 8(a).

Figure 8(b) and (c) shows images of a mixture of oil droplets at the 1260 and 1300 cm^{-1} peaks, respectively. The images are constructed by integrating from 1220 to 1282 cm^{-1} for Fig. 8(b) and from 1282 to 1344 cm^{-1} for Fig. 8(c). The power of the pump,

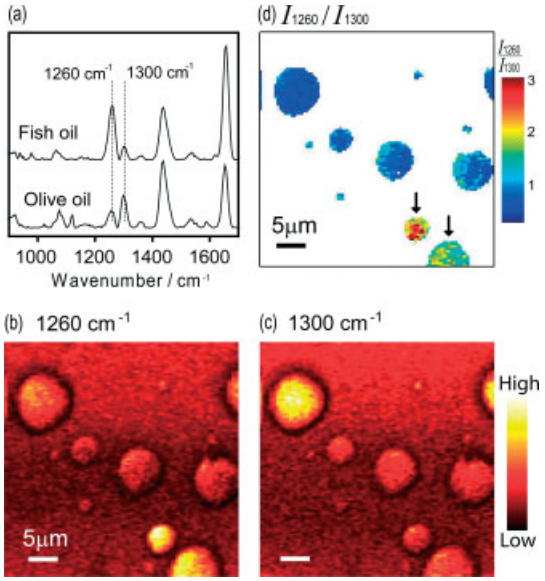

Figure 8. (a) FTSI-CARS spectra of fish and olive oil. (b)–(d) CARS images of a mixture of olive and fish oil droplets. Images are constructed with peaks at (b) 1260 cm^{-1} and (c) 1300 cm^{-1}, respectively. The images have 100 × 100 pixels and the pixel size is 300 nm × 300 nm^2. The total image acquisition time is 3.4 s. (d) Intensity ratio (I_{1260}/I_{1300}) image of 1260 cm^{-1} and 1300 cm^{-1} peaks. The only area with significant intensity at 1450 cm^{-1} is shown in color. Fish oil droplets are marked with arrows. Other droplets are of olive oil.

Stokes, and probe pulses are 4.8, 2.4, and 0.3 mW, respectively. The image acquisition speed is 3.4 s per frame. Droplets with a higher intensity in Fig. 8(b) and (c) are fish and olive oils, respectively. Figure 8(d) shows the map of I_{1260}/I_{1300}. One can clearly identify each droplet by the peak intensity ratio. Fish oil droplets are marked with arrows in Fig. 8(d).

As demonstrated in this work, our FTSI-CARS method can provide great chemical selectivity via analysis of multiple vibrational peaks. It can obtain a vibrational hyperspectral image within a few seconds. The apodization function introduced in the signal retrieval process eliminated background other than shot noise. This technique can be an excellent chemical imaging tool for material and food samples. It will be especially useful in quantification of different fat contents in food products.

Conclusion

In this work, we presented the improvements in both sensitivity and imaging speed of the FTSI-CARS microscopy method. We showed that the spectral noises from the etalon effect of back-illuminated CCD and non-flat transmission spectrum of the laser-blocking filter can be removed in the signal normalization step. The background originating from laser drift and/or different spectral shape of nonresonant background could be eliminated by introducing the time apodization function instead of the Heaviside step function in the FTSI signal retrieval process. We experimentally verified that the sensitivity of our CARS technique is nearly shot-noise-limited. The detection sensitivity limit of aqueous sulfate ions is ~10 mM in 2 s, which corresponds to 1.2×10^6 oscillators in the effective laser focal volume. The FTSI-CARS signal shows a linear dependence on the sample concentration, confirming the signal amplification by nonresonant background. Accompanied by the crop mode operation of CCD, we can now obtain a hyperspectral

vibrational image of 100 × 100 pixels in 3 s and a 3D image of 100 × 100 × 50 pixels in 3 min. Chemically, selective microscopy of heterogeneous samples such as mixtures of polymers and oil droplets is successfully demonstrated. This technique can be a powerful microscopy tool for probing a local chemical identity in highly inhomogeneous samples.

Acknowledgements

The authors gratefully acknowledge the Welch Foundation for the support of personnel (project F-1663).

References

[1] J.-X. Cheng, X. S. Xie, *J. Phys. Chem. B* **2004**, *108*, 827.
[2] C. L. Evans, X. S. Xie, *Annu. Rev. Anal. Chem.* **2008**, *1*, 883.
[3] J.-X. Cheng, *Appl. Spectrosc.* **2007**, *61*, 197A.
[4] E. O. Potma, X. S. Xie, L. Muntean, J. Preusser, D. Jones, J. Ye, S. R. Leone, W. D. Hinsberg, W. Schade, *J. Phys. Chem. B* **2004**, *108*, 1296.
[5] M. Müller, A. Zumbusch, *Chemphyschem* **2007**, *8*, 2157.
[6] A. Zumbusch, G. R. Holtom, X. S. Xie, *Phys. Rev. Lett.* **1999**, *82*, 4142.
[7] F. Ganikhanov, C. L. Evans, B. G. Saar, X. S. Xie, *Opt. Lett.* **2006**, *31*, 1872.
[8] C. L. Evans, E. O. Potma, M. Puoris'haag, D. Côté, C. P. Lin, X. S. Xie, *Proc. Natl. Acad. Sci. U.S.A.* **2005**, *102*, 16807.
[9] T. Hellerer, C. Axäng, C. Brackmann, P. Hillertz, M. Pilon, A. Enejder, *Proc. Natl. Acad. Sci. U.S.A.* **2007**, *104*, 14658.
[10] J.-X. Cheng, S. Pautot, D. A. Weitz, X. S. Xie, *Proc. Natl. Acad. Sci. U.S.A.* **2003**, *100*, 9826.
[11] H. Wang, Y. Fu, P. Zickmund, R. Shi, J.-X. Cheng, *Biophys. J.* **2005**, *89*, 581.
[12] X. Nan, E. O. Potma, X. S. Xie, *Biophys. J.* **2006**, *91*, 728.
[13] H. A. Rinia, N. J. Burger, M. Bonn, M. Muller, *Biophys. J.* **2008**, *95*, 4908.
[14] S.-H. Lim, A. G. Caster, S. R. Leone, *J. Phys. Chem. B* **2006**, *110*, 5196.
[15] B.-C. Chen, S.-H. Lim, *J. Phys. Chem. B* **2008**, *112*, 3653.
[16] J.-X. Cheng, A. Volkmer, L. D. Book, X. S. Xie, *J. Phys. Chem. B* **2002**, *106*, 8493.
[17] T. W. Kee, M. T. Cicerone, *Opt. Lett.* **2004**, *29*, 2701.
[18] K. P. Knutsen, B. M. Messer, R. M. Onorato, R. J. Saykally, *J. Phys. Chem. B* **2006**, *110*, 5854.
[19] S.-H. Lim, A. G. Caster, S. R. Leone, *Opt. Lett.* **2007**, *32*, 1332.
[20] M. Müller, J. M. Schins, *J. Phys. Chem. B* **2002**, *106*, 3715.
[21] D. Oron, N. Dudovich, Y. Silberberg, *Phys. Rev. Lett.* **2002**, *89*, 273001.
[22] D. Oron, N. Dudovich, Y. Silberberg, *Phys. Rev. Lett.* **2003**, *90*, 213902.
[23] M. Bonn, M. Müller, H. A. Rinia, K. N. J. Burger, *J. Raman Spectrospc.* **2009**, *40*, 763.
[24] D. Schafer, J. A. Squier, J. van Maarseveen, D. Bonn, M. Bonn, M. Müller, *J. Am. Chem. Soc.* **2008**, *130*, 11592.
[25] M. Cui, M. Joffre, J. Skodack, J. P. Ogilvie, *Opt. Express* **2006**, *14*, 8448.
[26] D. L. Marks, S. A. Boppart, *Phys. Rev. Lett.* **2004**, *92*, 123905.
[27] T. W. Kee, H. Zhao, M. T. Cicerone, *Opt. Express* **2006**, *14*, 3631.
[28] Y. Liu, Y. J. Lee, M. T. Cicerone, *J. Raman Spectrospc.* **2009**, *40*, 726.
[29] J. Sung, B.-C. Chen, S.-H. Lim, *Opt. Lett.* **2008**, *33*, 1404.
[30] M. D. Levenson, S. S. Kano, *Introduction to Nonlinear Laser Spectroscopy*, Academic Press, Inc.: San Diego, CA, **1988**.
[31] M. Butler, N. Salem, W. Hoss, J. Spoonhower, *Chem. Phys. Lipids* **1979**, *24*, 99.
[32] J. R. Beattie, S. E. J. Bell, B. W. Moss, *Lipids* **2004**, *39*, 407.